Biophysical Journal
Biophysical perspective

Biophysical Society

Iterative annealing mechanism for protein and RNA chaperones

Changbong Hyeon[1,*] and D. Thirumalai[2,*]
[1]Korea Institute for Advanced Study, Seoul, Korea and [2]Department of Chemistry, University of Texas at Austin, Austin, Texas

ABSTRACT Molecular chaperones are machines that consume copious amounts of ATP to facilitate the folding of misfolded proteins or RNA to their functionally competent native states by driving them out of equilibrium. Because the folding landscapes of biomolecules with complex native state topology are rugged, consisting of multiple minima that are separated by large free energy barriers, folding occurs by the kinetic partitioning mechanism according to which only a small fraction of the molecules reach the folded state in biologically viable times. The remaining fraction is kinetically trapped in a manifold of misfolded states. Folding of such recalcitrant proteins and RNA requires chaperones. Although the protein and RNA chaperones are profoundly different in their structure and action, the principles underlying their activity to produce the folded structures can be understood using a unified theoretical framework based on iterative annealing mechanism. Our theory, which quantitatively explains a number of experimental data, shows that both these machines have evolved to maximize the steady-state yield on biological times. Strikingly, the theory predicts that only at a moderate level of RNA chaperone activity is the yield of the self-splicing pre-RNA maximized in vivo.

SIGNIFICANCE Proteins and RNA that do not fold spontaneously with sufficient yield require molecular chaperones to reach the native structures. ATP-consuming molecular machines GroEL and CYT-19, respectively, facilitate the production of functionally competent proteins and group I intron. Although the molecular mechanisms of their functions are dramatically different, the theory based on the iterative annealing mechanism provides a quantitative description of the outcomes of experiments. The iterative annealing mechanism postulates that chaperones utilize the free energy of ATP hydrolysis to rescue misfolded structures by providing multiple opportunities to fold. By operating under nonequilibrium conditions, both GroEL and CYT-19 have evolved to maximize the yield of the folded state on biological times.

INTRODUCTION

The thermodynamic hypothesis, formulated by Anfinsen (1,2), asserts that the information needed to spontaneously reach the unique three-dimensional (3D) folded states of proteins is fully encoded in the primary sequence (1). In other words, protein folding is a self-assembly process. This expectation is borne out in numerous in vitro experiments on proteins with simple topologies and is the basis of structure prediction (3) and protein design (4). In addition to the uniqueness of the native fold, rapid folding kinetics could be important for sustaining high fidelity of biological functions, as already implied by experiments showing the recovery of RNaseA activity upon urea denaturation and subsequent renaturation upon depleting urea (5). However, not all proteins fold spontaneously (6,7) with sufficient yield. Such proteins are either long and/or their folded states have complex topologies. As a result, they are kinetically trapped in deep minima from which transition to the folded state takes place on timescales that are too long to be biologically viable.

Trapping in metastable native-like states is a lot more common in RNA than in proteins. Indeed, the folding kinetics of even RNA with simple architecture, such as hairpins, occurs in stages that is explained by the tendency to populate multiple intermediates (8,9). In general, a typical spectrum of RNA shows that there are several low-lying excitations that are easily accessible from the folded state. The free energy barriers separating such states from the folded state in ribozymes are large. Consequently, the transition times from the misfolded to the folded state could be hours or longer (10,11). The rescue of such recalcitrant proteins and RNA requires molecular chaperones, which likely evolved over a billion or more years ago, in bacteria (12).

The purpose of this article is to synthesize experimental and theoretical developments to create a unified framework,

Submitted June 14, 2025, and accepted for publication October 9, 2025.
*Correspondence: hyeoncb@kias.re.kr or dave.thirumalai@gmail.com
Editor: Alexandra Zidovska.
https://doi.org/10.1016/j.bpj.2025.10.016

based on the iterative annealing mechanism (IAM) (6,13), to understand the action of protein and RNA chaperones. For concreteness, we focus on the *Escherichia coli* GroEL/ES machinery (referred to as chaperonins) and the seemingly unrelated RNA enzyme CYT-19. Although both of these systems have been separately investigated (14–18), there are only a handful of works (19–23) that have provided a common description by invoking nonequilibrium mechanisms. Let us briefly introduce these two molecular machines. 1) Although the identities of the proteins that are helped by GroEL, belonging to the heat shock family HSP60, during the cell cycle, are not precisely known, it appears that only a small percent of the *E. coli.* proteome (24) may recruit the GroEL machinery to assist in the folding process. It is worth noting that assisted folding occurs without violating the tenets of the Anfinsen hypothesis. In other words, the sequence encodes the topology of the folded structure as well as the folding mechanism. We hasten to add that the possibility of chaperone redundancy implies that the fraction of proteins that are helped by chaperones could be larger than estimated previously (24). Given the rate of polypeptide synthesis *E. coli.* is substantial (≈60,000 chains/s (24)), it is unlikely that all of them could be chaperoned to the folded state, especially considering the mechanisms used by various chaperones are different.

Importantly, GroEL is a promiscuous machine that assists the folding of proteins whose native states are structurally unrelated (25), implying it is blind to the architecture of the folded proteins. 2) That proteins can facilitate the folding of RNA has been known over 40 years thanks to a pioneering, but often overlooked, study (26), which showed that tRNA could be reconstituted upon addition of proteins that potentially bind to single-stranded regions of RNA, which are presumably exposed in the misfolded states. More recently, it has been shown definitely that the ATP-consuming DEAD-box protein CYT-19, found in *Neurospora crassa* and the related Mss 116 in yeast, has chaperone activity (27,28). Importantly, the absence of CYT-19 in mutants of *Neurospora crassa* resulted in the accumulation of misfolded states of group I intron. Like GroEL, the fungi-derived CYT-19 is also promiscuous in the sense that it exhibits chaperone activity toward RNA from other organisms (27,29). Despite considerable differences between these two machines, which we explain below, the IAM provides a single unified framework that quantitatively explains all the available experiments and provides a platform to anticipate universal features of chaperone activity.

THEORETICAL BACKGROUND

Kinetic partitioning mechanism

The need for chaperones is illustrated by considering spontaneous folding of RNA and proteins with complex topology. The folding landscapes of these biomolecules are rugged (30–33), consisting of multiple minima separated by large free energy barriers that are difficult to cross in biologically relevant times. The conformations in the ensemble of misfolded states are frustrated. There are two sources of frustration. Energetic frustration is one, arising from competing interactions between distinct arrangements of the amino acid residues (6,34–36) (or nucleotides (37)). As a result, not all favorable interactions at a specific residue or a nucleotide location can be simultaneously satisfied (6,37). On the other hand, the more severe topological frustration (30,38) is caused by the incompatibility between stable structures formed on local length scales and the global native fold. The structures in the topologically frustrated states have strong similarity to the native state (38,39). Because of the rough free energy landscape, long-lived misfolded native-like metastable states readily form during the folding reaction. This is indeed the case in the folding of Rubisco (6,40) and *Tetrahymena* ribozyme (10).

The kinetic partitioning mechanism (KPM), which follows from the description of the rugged folding landscape, provides a unified theory (6,30,37–39) to describe folding of both RNA and proteins under nonpermissive conditions in which the yield of the folded state is paltry. According to KPM, only a small fraction, Φ, of molecules reaches the native state. The remaining fraction is trapped in one of the many minima for arbitrarily long times. The nonconvexity of folding landscape engenders multiple parallel folding pathways, giving rise to folding kinetics that are best fit to a multiexponential function,

$$P_N(t) = 1 - \Phi e^{-t/\tau_f} - \sum_i \phi_{s,i} e^{-t/\tau_{s,i}}. \quad (1)$$

Here, τ_f is the time for reaching the native state by the fast route, and $\phi_{s,i}$ and $\tau_{s,i}$ are those associated with slow routes. It should be stressed that the relations $\tau_{s,I} \gg \tau_f$ are satisfied. Conservation of flux implies that $\Phi + \sum_i \phi_{s,i} = 1$ should be satisfied.

For small, fast-folding globular proteins, $\tau_f \sim \mathcal{O}(1)$ ms and $\Phi \approx 1$. However, this is not the case for proteins with complex topology, whose folding landscape is rugged, as illustrated in Fig. 1. Navigation in such a landscape gives rise to predominantly slow track trajectories whose kinetics is best described by the KPM (Eq. (1)). With the assumption that the ensemble of folding intermediates satisfies the condition $\sum_i \phi_{s,i} = 1 - \Phi$ and $\tau_{s,I} \approx \tau_s$, $P_N(t)$ in Eq. (1) simplifies as

$$\begin{aligned} P_N(t) &\approx 1 - \Phi e^{-t/\tau_f} - (1 - \Phi) e^{-t/\tau_s} \\ &\rightarrow \Phi\left(1 - e^{-t/\tau_f}\right). \end{aligned} \quad (2)$$

The expression after the arrow, describing the transition from misfolded intermediates, to the native state is prohibitively long, $\tau_s \gg \tau_f$. In this case, even if the stability of the native state is far greater than the intermediate state, $\Delta G_{MN} = G_N - G_M \ll 0$, direct transitions from the misfolded

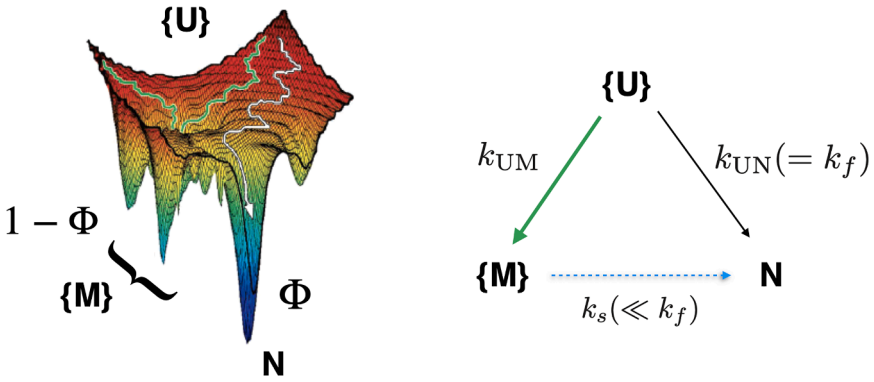

FIGURE 1 Rugged folding landscape and the kinetic partitioning mechanism (38), highlighting the multiple parallel pathways to the native state (N). The ensembles of unfolded states and folding intermediates are denoted by $\{U\}$ and $\{M\}$, respectively. The yield of the folded state of the fast-track molecules (*white path*) is quantified by the partition factor Φ. The green lines are the slow trajectories. The fast trajectory in white with an arrow reaches the folded state without being kinetically trapped in a deep local minimum. The three-state reaction scheme on the right simplifies the KPM, thus enabling an analytical solution to the kinetic model (38).

intermediates to the native state are effectively forbidden on a biologically relevant time or on in vitro timescales. As a result, $\Phi(1-e^{-t/\tau_f})\rightarrow\Phi$ for $t\gg\tau_f$, and only the fraction Φ of the entire population reaches the native state.

By assuming that the folding landscape in Fig. 1 may be mapped onto a three-state model consisting of $\{U\}$, $\{M\}$, and N, the "partition factor," Φ, is determined by the ratio of initial collapse rates of an ensemble of unfolded conformations ($\{U\}$) to the native state (N) and misfolded intermediates ($\{M\}$),

$$\Phi = \frac{k_{\mathrm{UN}}}{k_{\mathrm{UM}} + k_{\mathrm{UN}}}. \tag{3}$$

We note that $\{U\}$ can be replaced with $\{I\}$, a notation used in our studies on RNA (19,23), where it was made explicit that the initial state of IAM corresponds to an ensemble of collapsed intermediates that could contain residual secondary structures, instead of fully unfolded states. Once trapped in long-lived kinetic intermediates in which the hydrophobic patches are not fully sequestered to the interior of the structure, functionally incompetent misfolded proteins could accumulate, potentially forming protein aggregates, which are likely to be deleterious the cell. Similarly, errors in basepairing or incorrect topological arrangement of reformed helices would result in metastable states with long lifetimes.

Several in vitro experiments on RNA and proteins have been interpreted in terms of the KPM. 1) Folding of hen egg white lysozyme near room temperature and neutral pH showed that $\Phi = 0.15$ (7) can be increased to $\Phi = 0.25$ (41) by changing pH. The partition factor Φ can be increased or decreased not only by changing the external conditions but all also by mutations (42,43). 2) The value of Φ for Rubisco is (0.02–0.05) (44), which makes it a stringent substrate for GroEL. 3) The first ensemble experimental measurements on *Tetrahymena* ribozyme showed that $\Phi \approx 0.08$ (10), which was subsequently confirmed in single-molecule experiments (45). Interestingly, upon stabilization of a point mutation that stabilized the P3 pseudoknot using a single point mutation increases by a factor of eight (42).

GroEL-GroES machinery

To facilitate folding and maintain protein homeostasis, cells overexpress molecular chaperones, particularly under conditions that trigger aggregation, such as during heat shock. Although first known in the context of genetics of bacteriophage assembly and the synthesis of the large subunit of ribulose-1,5-bisphosphate carboxylase/oxygenase (Rubisco) over 40 years ago (46,47), it was only in the late 1980s (48,49) that it became clear that GroEL-GroES machinery is involved in the rescue of heterologously expressed proteins. GroEL is a barrel-shaped heptameric oligomer with a sevenfold symmetry with a large central cavity (50), which naturally suggests that the substrate protein is merely sequestered in the Anfinsen cage till the native state is reached (51,52). Recent developments have demonstrated that the neither the passive nor the active cage Anfinsen model, which argues that the protein folding rate is accelerated by confinement effects (53,54), is relevant in the function of GroEL. Several experiments support the theory based on IAM. 1) When challenged with a misfolded substrate protein and supply of ATP, the GroEL machinery springs to action by undergoing large conformational changes, by twisting the barrel and doubling the volume of the central cavity (55,56). These allosteric transitions, requiring ATP binding and hydrolysis (57,58), are required in helping proteins fold, implying the GroEL/ES plays an active role in its function. 2) Furthermore, ATP binding and hydrolysis exert mechanical stress to the encapsulated proteins, which destabilizes the misfolded proteins (59–61). 3) Thanks to experiments from several laboratories, it is now firmly established that the symmetric (or "American football") complex is the functional unit (40,62–69). These experiments show that when challenged with substrate proteins the GroEL/ES becomes a parallel processing machine, discharging all the ligands with each round of the catalytic cycle, maximizing the number of

iterations (by minimizing the residence time of the substrate proteins in the cavity), thus enhancing the production of the native material, as predicted by the IAM (see below).

The action of GroEL conformation on the $(1-\Phi)$ population of misfolded proteins ($\{M\}$) is to unfold (at least partially) (70) the conformations in the $\{U\}$ state and offer another chance to refold. It is worth noting that when encapsulated in the cavity, the substrate protein undergoes partitioning rapidly, either to the folded or to one of the misfolded states, on timescales that are less than substrate residence time in the Anfinsen cage. In other words, when the substrate protein folds, it does so in the cavity. In the second round of folding, $\Phi(1-\Phi)$ would fold to the native state, and the fraction, $(1-\Phi)^2$, would again misfold. When this process is repeated $n(=t/\tau_0)$ times, where τ_0 is the time associated with a single cycle of chaperone action, which has been shown to be $\tau_0 \approx 2$ s, and t is the time duration of the entire process, the fraction $(1-\Phi)^n$ still remains misfolded, which implies that the fraction $1-(1-\Phi)^n$ reaches the folded state. Thus, the yield of native state after n-cycle of chaperone action is obtained as

$$P_N(n) = 1-(1-\Phi)^n \xrightarrow[n=t/\tau_0]{\Phi \ll 1} 1-e^{-\Phi t/\tau_0}. \quad (4)$$

This is the gist of IAM of chaperone-assisted protein folding, which is reminiscent of the simulated annealing protocol (14) for solving the optimization problem in computer science (71) and the stochastic resetting in target-search processes (72,73). Then, if there are equal amounts of GroEL/ES chaperonin system and proteins in the cell, the time required for a GroEL/ES particle to produce the 100% population of native states of the Rubisco with $\Phi \approx 0.05$ is around 40 s.

Here, it is worth noting that the steady-state yield of native state is 100%, i.e., $P_N(n\to\infty) = 1$. The resulting situation is fundamentally different from an expectation based on the landscape picture at thermal equilibrium, where the native state yield should be dictated by the Boltzmann distribution, $P_N^{eq} = 1/(1+e^{-\Delta G_{MN}/k_BT})$. One might argue that for sufficiently large stability of the native state, $\Delta G_{MN} \ll 0$, such that folding landscapes are funneled, the native yield may be approximated to the unity ($P_N^{eq} \lessapprox 1$). However, the steady-state expression for the folded state using the theory based on the IAM does not coincide with the Boltzmann distribution, $P_N(n\to\infty) \neq P_N^{eq}$. Given that the operation of GroEL chaperonin cycle requires free energy consumption of ~(3–4) ATP molecules per cycle (65), the chaperone-assisted folding of proteins should be viewed as a far-from-equilibrium process where free energy is continuously injected and dissipated from the system (74–76). The distinction of $P_N(\infty)$ from P_N^{eq}, which may not immediately be clear for GroEL-assisted folding of a protein with large stability, is further clarified by discussing RNA chaperones whose action on RNA molecules is different from GroEL. RNA chaperones can destabilize the RNA conformation in the native state as well as the misfolded conformation. This aspect will be discussed in the next section.

RNA chaperones

Just like proteins, the folded state of RNA is encoded in the primary sequence. Although there are exceptions, it is thought that RNA folding is hierarchical that begins by first forming a secondary structure, followed by establishment of tertiary contacts between preformed secondary structural motifs (37). The catalytic (self-cleavage) activity of *Tetrahymena* ribozyme, which is one of the most extensively studied model systems for RNA folding, requires that it be folded correctly. However, experiments complemented by theoretical arguments based on KPM show that only $\Phi < 0.1$ for molecules reach the folded state spontaneously, which means that the majority of molecules are kinetically trapped (10). For instance, the partition factor Φ is as small as 0.08 during in vitro folding of *Tetrahymena* ribozyme (10). Incorrect formation of these structural motifs gives rise to a functionally incompetent ribozyme that compromises its cleavage activity. Fig. 3 *A* shows the two secondary structure maps of RNA. For this structure to properly self-assemble, five tertiary contacts between the preformed helices (indicated by aqua-colored arrows) should be correctly form (77–81). In particular, the pseudo knot formation, defined by the P3 helix, is critical. Without the P3 helix, the two major domains cannot be consolidated. Often during the folding process, an alternative helix (Alt-P3) is formed, resulting in a topological trap, whose corresponding structure is catalytically inactive (42).

Because Φ is small, folding of RNAs such as *Tetrahymena* ribozyme requires chaperones in vivo. DEAD-box protein CYT-19 is one of the general RNA chaperones, which belongs to superfamily 2 (SF2) helicase family, consisting of core helix domains and Arginine rich C-terminal tail (18,27,28,82,83). If RNA has surface-exposed helices or tertiary interaction motifs, as would be the case in the misfolded states, CYT-19 could recognize them and locally unwind the duplex into single strands. The unwinding process requires ATP consumption, which implies that CYT-19 activity is also a nonequilibrium process.

What distinguishes CYT-19 from GroEL is that CYT-19 can not only deactivate the native ribozyme but can also unwind the surface-exposed helices of the misfolded ribozyme (84). Under less stabilizing condition, ribozymes show low cleavage activity as a result of deactivation by CYT-19, and this trend is amplified at higher CYT-19 concentration (84). Such a scenario of deactivation of native state is not included in the IAM of GroEL in Fig. 2 because GroEL typically does not recognize the folded state. It was also found that the ribozyme at steady state ($t\to\infty$) in the presence of CYT-19 does not necessarily reach the unity as is predicted for GroEL-assisted folding yield of protein.

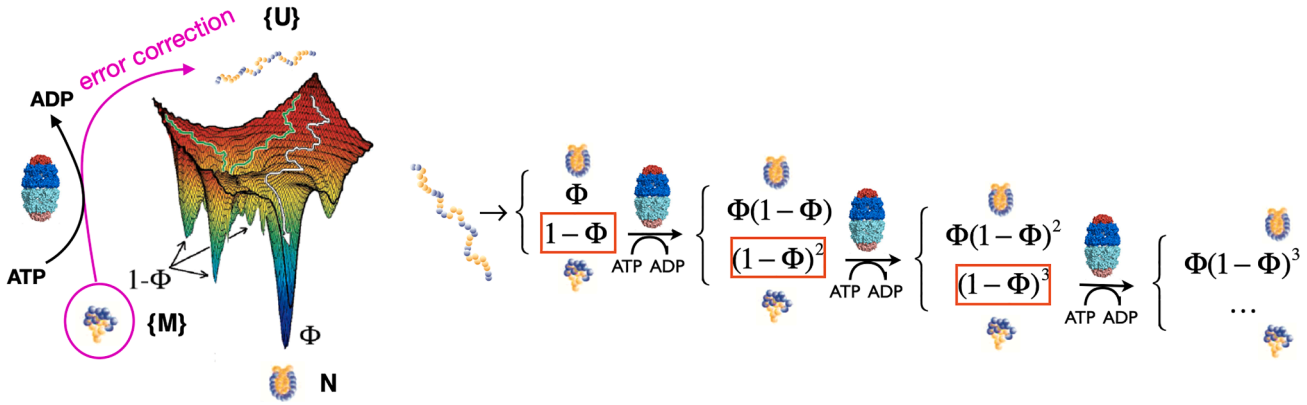

FIGURE 2 Changes in the subpopulations of protein while the protein conformations are iteratively annealed to their native state through the GroEL-GroES chaperonin-assisted folding. As illustrated, in the symmetric functional unit the substrate proteins can be present in both the chambers, thus making GroEL/ES a parallel processing machine. The residence time in the cavity is minimized in the presence of the substrate protein.

By considering the extent of chaperone-mediated disruption of native ribozyme relative to the misfolded ribozyme in terms of a factor κ ($0 \leq \kappa \leq 1$), one can follow a similar line of reasoning described previously (19,22,74) to derive the RNA chaperone-assisted folding yield of native ribozyme after the n-th round of chaperonin action:

$$P_N^{\kappa}(n) = \Phi \frac{1 - (1 - \kappa)^n (1 - \Phi)^n}{\kappa + (1 - \kappa)\Phi}. \tag{5}$$

This is the generalized expression of native yield by chaperone-assisted folding of biopolymers. The steady-state yield of the native state is give by

$$P_N^{\kappa}(\infty) = \frac{\Phi}{\kappa + (1 - \kappa)\Phi}. \tag{6}$$

Note that Eq. (4) is recovered by setting the factor $\kappa = 0$ in Eq. (5). In fact, the landscape model depicted in Fig. 3 *B* can be mapped onto the three-state kinetic model involving $\{U\}$, $\{M\}$, and N by incorporating the chaperone-mediated reverse transitions from $\{M\}$ to $\{U\}$ and from N to $\{U\}$, which are missing in Fig. 1. Such a model allows us to express the steady-state ($t \to \infty$ or $n \to \infty$) yield of native state in terms of the six rate constants. Furthermore, under the condition relevant to our discussion of chaperone-assisted folding of biopolymers, i.e., k_{NM}, $k_{\mathrm{MN}} \ll 1$, and $k_{\mathrm{UN}} \gg k_{\mathrm{NU}}$, it is straightforward to obtain,

$$P_N^{\kappa}(\infty) \approx \frac{k_{\mathrm{UN}}}{\left(\frac{k_{\mathrm{NU}}([C],[T])}{k_{\mathrm{MU}}([C],[T])}\right) k_{\mathrm{UM}} + k_{\mathrm{UN}}}. \tag{7}$$

Inserting the expression of the partition factor Φ (Eq. (3)) into Eq. (6) gives $P_N^{\kappa}(\infty) \approx \frac{k_{\mathrm{UN}}}{\kappa k_{\mathrm{UM}} + k_{\mathrm{UN}}}$. Thus, the factor κ is the ratio of chaperone-induced unfolding rate from native and misfolded state:

$$\kappa = \frac{k_{\mathrm{NU}}([C],[T])}{k_{\mathrm{MU}}([C],[T])}, \tag{8}$$

where $[C]$ and $[T]$ are the chaperone and ATP concentrations, respectively, thus making it explicit that chaperone-induced unfolding rates depend on $[C]$ and $[T]$.

Although the expression is simple, Eq. (7) along with Eq. (8) is of great significance. First, steady-state yield of native state is less than one unless κ is zero, which is consistent with measurements (84). Second, the relative disruption factor κ is the ratio of two unfolding transition rates, both of which depend on the concentrations of chaperone and ATP. In the absence of ATP or chaperone (k_{NU}, $k_{\mathrm{MU}} = 0$), the majority of *Tetrahymena* ribozymes ($1 - \Phi \approx 0.92$) are trapped in the misfolded conformations devoid of catalytic power. Given that ~100 ATP molecules are consumed by the action of RNA chaperone to fully refold a single misfolded ribozyme (23,83), one cannot stress enough the outcomes arising from the energy-expending, nonequilibrium nature of chaperone-assisted folding. This key prediction of the theory is a manifestation of the non-Boltzmann steady-state yield of native state ($P_N^{ss} \neq P_{eq}^N$), violation of detailed balance, and generation of nonvanishing reaction current in the three-state kinetic model (see Ref. (19) for the further details).

We note that the three-state model discussed here may be extended to include multiple misfolded state ensembles, such that the $\{M\}$ ensemble can be further classified as $\{M_1\}$, $\{M_2\}$, … states, to be consistent with the experimental classifications of *Tetrahymena* ribozyme, as have been analyzed in Ref. (23) (see Figure 3 and Table 2 therein). For the model with m misfolded state ensembles and a unique native state, the expressions for Φ and κ can straightforwardly be extended to

$$\Phi = \frac{k_{\mathrm{UN}}}{k_{\mathrm{UN}} + \sum_{i=1}^{m} k_{\mathrm{UM_i}}} \tag{9}$$

and

$$\kappa = \frac{k_{\mathrm{NU}}([C],[T])}{\sum_{i=1}^{m} k_{\mathrm{M_iU}}([C],[T])}. \tag{10}$$

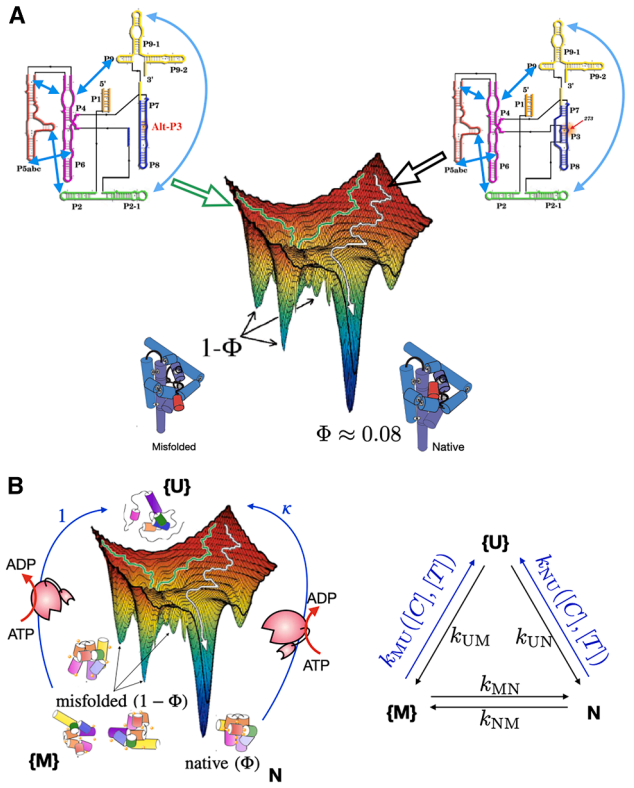

FIGURE 3 Kinetic paritioning mechanism of RNA folding and iterative annealing mechanisms by RNA chaperones. (*A*) Illustration of in vitro folding of *Tetrahymena* ribozyme via kinetic partitioning. One of the major causes of misfolding due to the formation of Alt-P3 helix in the secondary structure is highlighted together with the differing pathways on the folding landscape. The partition factor is only $\Phi \approx 0.08$. (*B*) A folding landscape highlighting the role of ATP-burning RNA chaperone, CYT-19, and its mapping onto the three-state kinetic model. Illustration of in vitro folding of *Tetrahymena* ribozyme via kinetic partitioning. One of the major causes of misfolding is the formation of Alt-P3 helix in the secondary structure, which is highlighted together with the differing pathways on the folding landscape. The partition factor is only $\Phi \approx 0.08$. A folding landscape showing the role of ATP-burning RNA chaperone, CYT-19, and its mapping onto the three-state kinetic model.

The inclusion of multiple states comes at the expense of several additional parameters, which would be hard to determine experimentally. Our previous study has shown that the three-state model accurately explains the experimental data (19).

RNA folding in cells

Self-splicing reaction involving the removal of the noncoding intron occurs in the absence of proteins. However, RNA must be folded, which as described above requires DEAD-box proteins. To account for RNA folding and the splicing reaction simultaneously, we created a theory (23) by extending the IAM to assess the effect of RNA chaperone on the yield of the self-spliced pre-RNA (*SP*), which is the main product of the catalytic activity of the group I intron *Tetrahymena* ribozyme (Fig. 4 *A*). Fig. 4 *B* shows the kinetic network that describes the interplay between the folding dynamics of *Tetrahymena* ribozyme, chaperone-mediated unfolding, and self-splicing reactions as well as the degradation of the transcript. Pre-RNA, synthesized during transcription, first reaches the *I* state, followed by folding to the *N* state or misfolding to the *M* state of the ribozyme, as described by the KPM. Self-splicing of the catalytically competent state of ribozyme ensues to yield the state denoted by *SP*. The self-splicing rate (k_s) is typically greater than the folding rates (85,86). Moreover, folding rate is much faster than the degradation rates ($k_d \ll k_{IM}$, $k_{IN} \ll k_s$), which is assumed to be independent of the RNA conformation. Let the chaperone-mediated unfolding be k_{MI}^{eff} and k_{NI}^{eff}. Given that the transitions between *M* and *N* states are prohibitively slow, $k_{NM} \ll 1$ and $k_{MN} \ll 1$, the expression of the steady-state population of SP (P_{SP}^{ss}) is straightforward to derive, as described in detail in the supporting material given in our theory (23).

Fig. 4 *C* shows the chaperone activity-dependent steady-state yield of P_{SP}^{ss} for various values of the relative disruption factor, κ. Of particular note is that for $\kappa \neq 0$, P_{SP}^{ss} varies non-monotonically with the unfolding activity of RNA chaperones (k_{MI}^{eff}), reaching a maximum at

$$k_{MI}^{eff} \approx \sqrt{\frac{k_{IM} k_s}{\kappa}}, \tag{11}$$

which is equivalent to $k_{MI}^{eff} k_{NI}^{eff} \approx k_{IM} k_s$. This shows that RNA splicing is maximized only at a moderate level of RNA chaperone activity. To attain the maximum yield of *SP*, the chaperone activity should be large enough to rescue pre-RNA from the misfolded states ($k_{MI}^{eff} > k_{IM}$), whereas the chaperone-mediated unfolding of native state must not overwhelm the rate of splicing ($k_{NI}^{eff} < k_s$).

DISCUSSION

Nonequilibrium effects

We showed previously that the steady values of the yield of the native states of CYT-19 mediated folding of *Tetrahymena* ribozyme and its variant as well as GroEL-assisted reconstitution of Rubisco and malate dehydrogenase (MDH) do not approach the Boltzmann distribution (see Figs. 4–6 in (19)). This implies that chaperones drive the substrate population out of equilibrium (19), thus increasing the accessibility of the native state on a biologically relevant timescale. What matters for the cellular function is that the supply rate of native enzyme production (P_N/τ) must match the cellular demand, not the yield of native state (P_N) per se. The situation is analogous to the tradeoff between efficiency of heat engines (Carnot engine for example) and generation of maximal power. Although maximum Carnot efficiency is achieved when operated under quasi-static conditions, power generation would be compromised. From

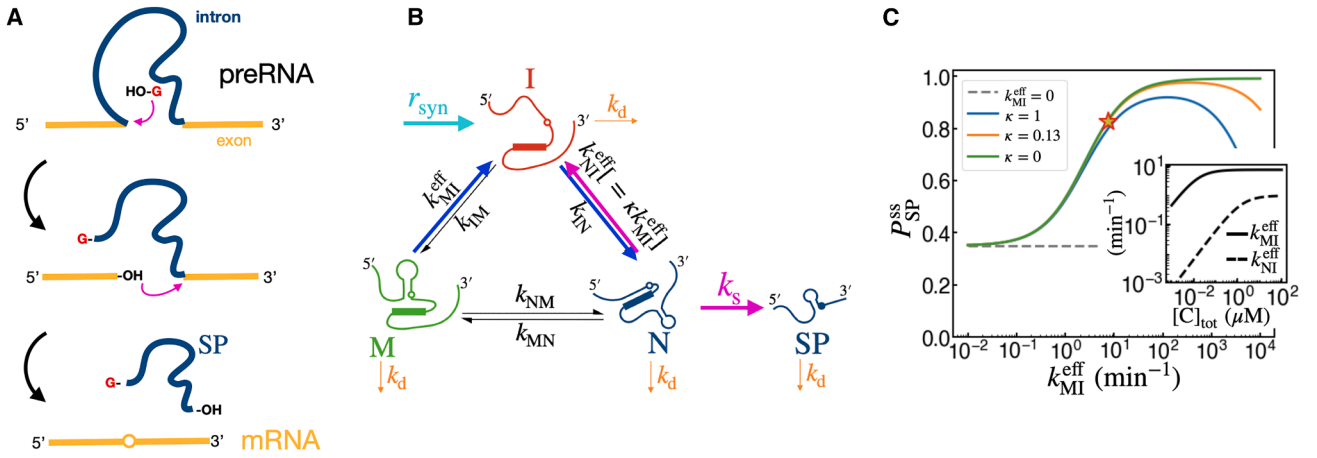

FIGURE 4 Effect of RNA chaperone on the self-splicing yield of preRNA. (*A*) Schematic of group I intron splicing of preRNA leading to the production of mRNA transcript. (*B*) Kinetic network model combining chaperone-mediated folding and the self-splicing of pre-RNA. RNA degradation rate is k_d that could occur from all the relevant states. Experiments (27,85,86) suggest that k_s is greater than $k_{I\to M}$ and $k_{I\to N}$ and $k_d < k_{I\to M}, k_{I\to N} < k_s$ where k_s is the splicing rate. (*C*) The yield of the self-spliced preRNA as a function of chaperone activity ($k_{\text{eff}}^{\text{MI}}$), at different values of the recognition factor, κ. The rate constants ($k_{I\to M}$, $k_{M\to N}$, $k_{N\to M}$, k_d, and k_s) used in the kinetic model (*B*) are listed in the caption to Fig. 5 *B* in (23). The star symbol is evaluated at $k_{\text{MI}}^{\text{eff}} \approx 7.5\ \text{min}^{-1}$ (the saturation value in inset) with $\kappa = 0.13$.

the perspective of power generation, it is more important to operate the engine at a fast rate (nonequilibrium conditions) than in the quasi-static limit where the thermodynamic efficiency is maximized, with zero power. This well-known concept (power-efficiency tradeoff), in macroscopic heat engines, is also valid in microscopic engines in a stochastic fluctuating environment (74,87–89), and it is also found in the function of chaperones, which existed several billions years (12) before manmade steam engines were invented. It is clear that as long as cells tolerate misfolded enzymes (errors), execution of biological functions is determined by the production rate of catalytically active enzymes even at the expense of lavish consumption of ATP.

Chaperones solve an optimization problem

A general question that arises in the functions of biological motors is what is being optimized given the available resources in the cell (74). It is difficult to answer this question in complete generality because various biological machines have evolved at different periods to perform a myriad of totally unrelated functions. For instance, in the case of the well-studied molecular motors that ferry cargo (kinesin, myosin, and dynein) by walking on polar tracks, one could wonder if evolution has optimized processivity or speed. Although concepts from nonequilibrium statistical physics, especially thermodynamic uncertainty relations (75,90–92) and information theoretic approaches (93), have given insights, the answer might depend on the system under consideration. However, in the context of chaperones, one can make a clear prediction that is supported by experimental data. This is vividly illustrated in Fig. 5, which contrasts the steady-state yields of Rubisco and *Tetrahymena* ribozyme when the concentration of GroEL and CYT-19 is varied. In the presence of GroEL, which preferentially recognizes the misfolded states of proteins, the steady-state yield (P_N) of native Rubisco increases as the concentration of GroEL is increased. In sharp contrast, increase in the concentration of CYT-19 reduces P_N of the functional *Tetrahymena* ribozyme. The solution to the master equation (19,23) associated with the reversible three-state model (Fig. 3 *B*) indicates that these opposing trends originate from the distinct actions of the two chaperones on Rubisco and *Tetrahymena* ribozyme, which is quantified with different value of κ (Eq. (8)). The value of $\kappa \approx 0$ for GroEL on Rubisco, and $\kappa \approx 0.13$ for CYT-19 for *Tetrahymena* ribozyme (23). Strikingly, the IAM theory predicts that P_N/τ (τ is the longest relaxation time ($\approx$ the folding time) needed to reach the steady state) is an increasing function of the chaperone concentration for both GroEL and CYT-19 (Fig. 5 *B*). In other words, for a given concentration of chaperone, the product of the steady-state yield and the folding rate serves as a good indicator of the action of chaperone.

Lavish consumption of ATP

It is important to calculate the thermodynamic cost incurred in the process of annealing the structures. Both machines consume copious amounts of ATP in the process of rescuing misfolded structures. The theory shows about 125 ATP molecules are consumed to drive a single *Tetrahymena* ribozyme depending on the concentration of CYT-19 (23). Similarly, GroEL/ES systems burn between 60 and 120 ATP molecules in order to fold a single Rubisco molecule (6). Notwithstanding the argument that this is a mere fraction of the cost needed to synthesize the protein and RNA,

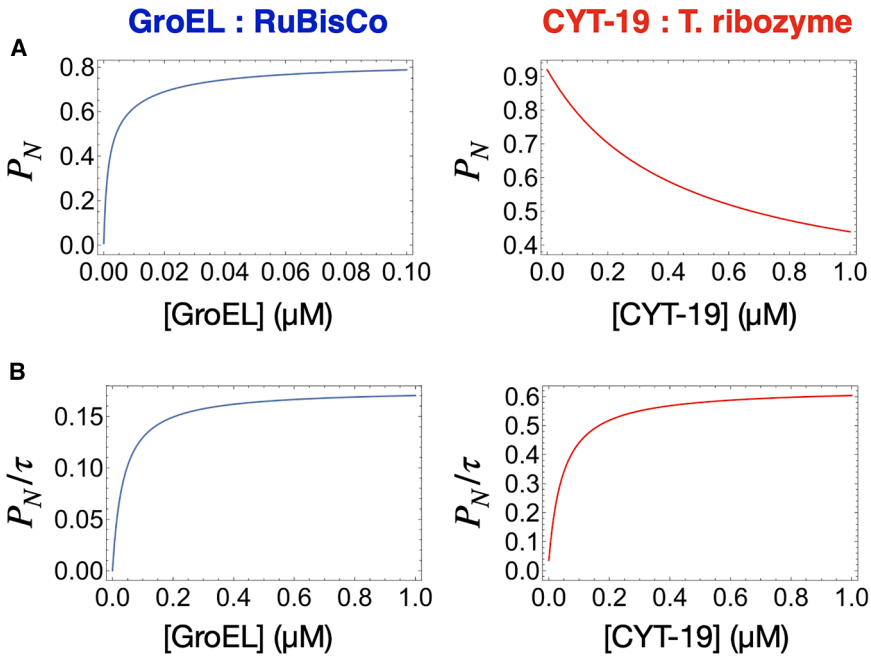

FIGURE 5 Maximization of finite time yield of the native state by chaperones. (*A*) Steady-state yield (P_N) of Rubisco (*left*) and *Tetrahymena* ribozyme (*right*) as a function of the corresponding chaperone concentration. (*B*) The steady-state yield per unit relaxation time of chaperone-assisted folding (P_N/τ) as a function of the chaperone concentration. In both cases, P_N/τ is an increasing function of the chaperone concentration in contrast to P_N in (*A*).

it has to be concluded that these machines are inefficient. These findings suggest that to maintain cellular homeostasis, minimization of error in protein and RNA functionality is prioritized over the high thermodynamic cost.

Evolutionary considerations

It is interesting to assess the potential evolutionary implications in light of several experiments (46,94,95). Of interest here are the early experiments, which showed that overexpression of GroEL facilitated assembly of heterologously expressed Rubisco subunits (96). Similarly, overexpression of GroEL/ES suppressed effects of temperature-sensitive mutants of coat protein (97), by enhancing folding efficiency and the stability of the protein, which could have been an early demonstration of nonequilibrium effects (19). More recently (98), using experiments combined with a kinetic model showed that chaperonins rescue the growth of *E. coli* deleterious DHFR mutants. In particular, the growth rate of the mutant strains was correlated with overabundance of folded DHFR, which in turn depended on GroEL/ES concentration. In formulating the IAM (6), we proposed that the GroEL/ES machinery could positively affect potentially deleterious effects of mutations. In case of deleterious mutations, the partition factor would decrease. The ability of chaperonins to rescue these conformers and allow them multiple chances to advance to the folded state explains experimental observations (96,97). In fact, RNA chaperones are also shown to contribute to the fitness of the host organism by reducing mutational load (99). Evolution also searches for new biological activities by mutating existing genes. In such cases, chaperonins would ensure that a mutant protein would explore the folding landscape by avoiding trapping in deep local minima. When sufficient mutations accumulate, an earlier kinetic trap could evolve to a new energy minimum with an altered function. These considerations suggest that chaperonins and the optimization of folding by IAM must have been a significant early evolutionary event.

CONCLUDING REMARKS

We have presented a common theoretical framework to quantitatively account for the functions (facilitate the folding of proteins and RNA that cannot do so spontaneously) of two seemingly unrelated molecular machines that must have appeared early in evolution. There are a couple of differences between GroEL/ES and CYT-19, the two chaperones used to illustrate the theory. 1) The annealing action of GroEL arises as a result of the changes in the microenvironment that the substrate protein experiences as result of ATP and GroES binding. Not only do these events double the volume of the central cavity, but the cavity changes from being hydrophobic before binding to hydrophilic after binding. It is the change in the microenvironment that serves as the mechanism of annealing action of GroEL. It is likely that our theory is applicable to the function of mitochondrial Hsp60, whose architecture is strikingly similar to GroEL/ES machine (100). 2) CYT-19 interacts with single-stranded or unstable regions of RNA, which occur readily when it misfolds. The helicase activity unfolds the helices in an ATP-dependent manner, thus

altering the folding landscape of the RNA. In this sense, CYT-19 is more actively engaged in interaction with misfolded structures than GroEL. During each catalytic cycle, the unfolding process places the RNA in different regions of the rugged folding landscape from which folding can commence anew. Unlike GroEL, the structural basis of ATP binding, hydrolysis rates, the mechanism of release of the RNA (folded or not), and the extent of processivity of the helicase are not known. 3) The most striking difference between the two machines lies in the interaction with the misfolded structures. GroEL predominantly recognizes only misfolded structures in which the hydrophobic residues are exposed. In sharp contrast, CYT-19 interacts with both misfolded as well as the native state. The less stable misfolded structures are recognized by CYT-19 with greater probability than the folded state.

Despite these differences, the theory based on the IAM quantitatively accounts for all the experimental observations (19). A striking prediction of the theory is that the action of protein and RNA chaperones may be universal in that they both maximize the native state yield on biological times by operating out of equilibrium. Importantly, extension of the theory predicts that, under cellular conditions, chaperone-mediated folding of group I intron ribozyme and the self-splicing reaction compete. Thus, the IAM theory predicts that to maximize the yield of the cleavage reaction, the chaperone should disrupt the conformations of the unfolded structures but not the native state before the splicing reactions. These two opposing requirements place bounds on the differences between the stabilities of the native and misfolded structures and the various kinetic rates in Fig. 4. Our prediction awaits experimental tests. Finally, we note that DEAD-box protein CsdA was shown to accelerate ribosome assembly by means of IAM (101), thus establishing the generality of the theory.

ACKNOWLEDGMENTS

We dedicate this paper to the memory of Erich Sackmamm, a brilliant biophysicist. Although E.S. had retired, he remained a teacher, exposing D.T. to several interesting problems in biophysics. We are also indebted to George H. Lorimer, Shaon Chakrabarti, and Xiang Ye for fruitful collaboration. C.H. thanks the Center for Advanced Computation in KIAS for providing the computing resources. D.T. was supported by a grant from the National Science Foundation (CHE 2320256), the Welch Foundation through the Collie-Welch Chair (F-0019), and the US-Israel Binational Grant (2021077).

AUTHOR CONTRIBUTIONS

C.H. and D. T. designed the research and wrote the article.

DECLARATION OF INTERESTS

The authors declare no competing interests.

REFERENCES

1. Anfinsen, C. B. 1973. Principles that govern the folding of protein chain. *Science.* 181:223–230.
2. Anfinsen, C. B., and H. A. Scheraga. 1975. Experimental and theoretical aspects of protein folding. *Adv. Protein Chem.* 29:205–300.
3. Jumper, J., R. Evans, …, D. Hassabis. 2021. Highly accurate protein structure prediction with AlphaFold. *Nature.* 596:583–589.
4. Huang, P.-S., S. E. Boyken, and D. Baker. 2016. The coming of age of de novo protein design. *Nature.* 537:320–327.
5. Anfinsen, C. B., R. R. Redfield, …, W. R. Carroll. 1954. Studies on the gross structure, cross-linkages, and terminal sequences in ribonuclease. *J. Biol. Chem.* 207:201–210.
6. Todd, M. J., G. H. Lorimer, and D. Thirumalai. 1996. Chaperonin-facilitated protein folding: Optimization of rate and yield by an iterative annealing mechanism. *Proc. Natl. Acad. Sci. USA.* 93:4030–4035.
7. Kiefhaber, T. 1995. Kinetic traps in lysozyme folding. *Proc. Natl. Acad. Sci. USA.* 92:9029–9033.
8. Hyeon, C., and D. Thirumalai. 2008. Multiple probes are required to explore and control the rugged energy landscape of RNA hairpins. *J. Am. Chem. Soc.* 130:1538–1539.
9. Kuznetsov, S. V., C. C. Ren, …, A. Ansari. 2008. Loop dependence of the stability and dynamics of nucleic acid hairpins. *Nucleic Acids Res.* 36:1098–1112.
10. Pan, J., D. Thirumalai, and S. A. Woodson. 1997. Folding of rna involves parallel pathways. *J. Mol. Biol.* 273:7–13.
11. Treiber, D. K., and J. R. Williamson. 1999. Exposing the kinetic traps in RNA folding. *Curr. Opin. Struct. Biol.* 9:339–345.
12. Viale, A. M., A. K. Arakaki, …, R. G. Ferreyra. 1994. Evolutionary relationships among eubacterial groups as inferred from groel (chaperonin) sequence comparisons. *Int. J. Syst. Bacteriol.* 44:527–533.
13. Hyeon, C., and D. Thirumalai. 2013. Generalized iterative annealing model for the action of RNA chaperones. *J. Chem. Phys.* 139:121924.
14. Thirumalai, D. 1994. Statistical Mechanics, Protein Structure, and Protein - Substrate Interactions, Chapter Theoretical Perspectives on in Vitro and in Vivo Protein Folding. Plenum, New York, pp. 115–134.
15. Woodson, S. A. 2010. Taming free energy landscapes with RNA chaperones. *RNA Biol.* 7:677–686.
16. Rajkowitsch, L., D. Chen, …, R. Schroeder. 2007. RNA chaperones, RNA annealers and RNA helicases. *RNA Biol.* 4:118–130.
17. Herschlag, D. 1995. RNA Chaperones and the RNA Folding Problem. *J. Biol. Chem.* 270:20871–20874.
18. Russell, R., I. Jarmoskaite, and A. M. Lambowitz. 2013. Toward a molecular understanding of RNA remodeling by DEAD-box proteins. *RNA Biol.* 10:44–55.
19. Chakrabarti, S., C. Hyeon, …, D. Thirumalai. 2017. Molecular Chaperones Maximize the Native State Yield on Biological Times by Driving Substrates out of Equilibrium. *Proc. Natl. Acad. Sci. USA.* 114:E10919–E10927.
20. Goloubinoff, P., A. S. Sassi, …, P. De los Rios. 2018. Chaperones convert the energy from ATP into the nonequilibrium stabilization of native proteins. *Nat. Chem. Biol.* 14:388–395.
21. Barducci, A., and P. De Los Rios. 2015. Non-equilibrium conformational dynamics in the function of molecular chaperones. *Curr. Opin. Struct. Biol.* 30:161–169.
22. Thirumalai, D., G. H. Lorimer, and C. Hyeon. 2020. Iterative annealing mechanism explains the functions of the GroEL and RNA chaperones. *Protein Sci.* 29:360–377.
23. Song, Y., D. Thirumalai, and C. Hyeon. 2022. Moderate activity of RNA chaperone maximizes the yield of self-spliced pre-RNA in vivo. *Proc. Natl. Acad. Sci.* 119:e2209422119.
24. Lorimer, G. H. 1996. A quantitative assessment of the role of the chaperonin proteins in protein folding in vivo. *FASEB J.* 10:5–9.

25. George, S., R. B. Bernard, …, D. Thirumalai. 2006. Residues in substrate proteins that interact with groel in the capture process are buried in the native state. *Proc. Natl. Acad. Sci. USA.* 103:4433–4438.
26. Karpel, R. L., and A. C. Burchard. 1980. Physical studies of the interaction of a calf thymus helix-destabilizing protein with nucleic acids. *Biochemistry.* 19:4674–4682.
27. Mohr, S., J. M. Stryker, and A. M. Lambowitz. 2002. A dead-box protein functions as an atp-dependent rna chaperone in group i intron splicing. *Cell.* 109:769–779.
28. Turcq, B., K. F. Dobinson, …, A. M. Lambowitz. 1992. A protein required for rna processing and splicing in neurospora mitochondria is related to gene products involved in cell cycle protein phosphatase functions. *Proc. Natl. Acad. Sci. USA.* 89:1676–1680.
29. Huang, H.-R., C. E. Rowe, …, P. S. Perlman. 2005. The splicing of yeast mitochondrial group I and group II introns requires a DEAD-box protein with RNA chaperone function. *Proc. Natl. Acad. Sci.* 102:163–168.
30. Thirumalai, D., and S. A. Woodson. 1996. Kinetics of Folding of Proteins and RNA. *Acc. Chem. Res.* 29:433–439.
31. Chen, S. J., and K. A. Dill. 2000. RNA folding energy landscapes. *Proc. Natl. Acad. Sci. USA.* 97:646–651.
32. Dill, K. A., and H. S. Chan. 1997. From Levinthal to pathways to funnels. *Nat. Struct. Biol.* 4:10–19.
33. Hyeon, C., and D. Thirumalai. 2003. Can Energy Landscape Roughness of Proteins and RNA be Measured by Using Mechanical Unfolding Experiments? *Proc. Natl. Acad. Sci. USA.* 100:10249–10253.
34. Bryngelson, J. D., and P. G. Wolynes. 1987. Spin glasses and the statistical mechanics of protein folding. *Proc. Natl. Acad. Sci. USA.* 84:7524–7528.
35. Wolynes, P. G., J. N. Onuchic, and D. Thirumalai. 1995. Navigating the folding routes. *Science.* 267:1619–1620.
36. Nymeyer, H., A. E. García, and J. N. Onuchic. 1998. Folding funnels and frustration in off-lattice minimalist protein landscapes. *Proc. Natl. Acad. Sci. USA.* 95:5921–5928.
37. Thirumalai, D., and C. Hyeon. 2005. RNA and Protein folding: Common Themes and Variations. *Biochemistry.* 44:4957–4970.
38. Guo, Z., and D. Thirumalai. 1995. Kinetics of Protein Folding: Nucleation Mechanism, Time Scales, and Pathways. *Biopolymers.* 36:83–102.
39. Thirumalai, D., D. K. Klimov, and S. A. Woodson. 1997. Kinetic partitioning mechanism as a unifying theme in the folding of biomolecules. *Theor. Chem. Acc.* 96:14–22.
40. Todd, M. J., P. V. Viitanen, and G. H. Lorimer. 1994. Dynamics of the chaperonin ATPase cycle: implications for facilitated protein folding. *Science.* 265:659–666.
41. Matagne, A., E. W. Chung, …, C. M. Dobson. 1998. The origin of the α-domain intermediate in the folding of hen lysozyme. *J. Mol. Biol.* 277:997–1005.
42. Pan, J., M. L. Deras, and S. A. Woodson. 2000. Fast Folding of a Ribozyme by Stabilization Core Interactions: Evidence for Multiple Folding Pathways in RNA. *J. Mol. Biol.* 296:133–144.
43. Sánchez, I. E., and D. U. Ferreiro. 2011. Gonzalo de Prat Gay. Mutational analysis of kinetic partitioning in protein folding and protein–dna binding. *Protein Eng. Des. Sel.* 24:179–184.
44. Tehver, R., and D. Thirumalai. 2008. Kinetic Model for the Coupling between Allosteric Transitions in GroEL and Substrate Protein Folding and Aggregation. *J. Mol. Biol.* 377:1279–1295.
45. Zhuang, X., L. E. Bartley, …, S. Chu. 2000. A single-molecule study of RNA catalysis and folding. *Science.* 288:2048–2051.
46. Friedman, D. I., E. R. Olson, …, F. Banuett. 1984. Interactions of bacteriophage and host macromolecules in the growth of bacteriophage lambda. *Microbiol. Rev.* 48:299–325.
47. Milos, P., and H. Roy. 1984. ATP-released large subunits participate in the assembly of RuBP carboxylase. *J. Cell. Biochem.* 24:153–162.
48. Golouginoff, P., A. A. Gatenby, and G. H. Lorimer. 1989. GroEL heat-shock proteins promote assembly of foreign prokaryotic ribulose bisphosphate carboxylase oligomers in Escherichia-Coli. *Nature.* 337:44–47.
49. Ostermann, J., A. L. Horwich, …, F. U. Hartl. 1989. Protein folding in mitochondria requires complex formation with hsp60 and ATP hydrolysis. *Nature.* 341:125–130.
50. Paul, B. S., Z. Xu, …, A. L. Horwich. 1998. Structure and function in groel-mediated protein folding. *Annu. Rev. Biochem.* 67:581–608.
51. Horwich, A. L., A. C. Apetri, and W. A. Fenton. 2009. The groel/groes cis cavity as a passive anti-aggregation device. *FEBS Lett.* 583:2654–2662.
52. Hofmann, H., F. Hillger, …, B. Schuler. 2010. Single-molecule spectroscopy of protein folding in a chaperonin cage. *Proc. Natl. Acad. Sci. USA.* 107:11793–11798.
53. Brinker, A., G. Pfeifer, …, M. Hayer-Hartl. 2001. Dual Function of Protein Confinement in Chaperonin-Assisted Protein Folding. *Cell.* 107:223–233.
54. Gupta, A. J., S. Haldar, …, M. Hayer-Hartl. 2014. Active cage mechanism of chaperonin-assisted protein folding demonstrated at single-molecule level. *J. Mol. Biol.* 426:2739–2754.
55. Thirumalai, D., and G. H. Lorimer. 2001. Chaperonin-mediated protein folding. *Annu. Rev. Biophys. Biomol. Struct.* 30:245–269.
56. Hyeon, C., G. H. Lorimer, and D. Thirumalai. 2006. Dynamics of allosteric transition in GroEL. *Proc. Natl. Acad. Sci. USA.* 103:18939–18944.
57. Horovitz, A., Y. Fridmann, …, O. Yifrach. 2001. Review:allostery in chaperonins. *J. Struct. Biol.* 135:104–114.
58. Horovitz, A., E. S. Bochkareva, …, A. S. Girshovich. 1994. Prediction of an Inter-residue Interaction in the Chaperonin GroEL from Multiple Sequence Alignment is Confirmed by Double-mutant Cycle Analysis. *J. Mol. Biol.* 238:133–138.
59. Korobko, I., R. B. Eberle, …, A. Horovitz. 2022. A diminished hydrophobic effect inside the GroEL/ES cavity contributes to protein substrate destabilization. *Proc. Natl. Acad. Sci.* 119:e2213170119.
60. Koculi, E., and D. Thirumalai. 2021. Retardation of folding rates of substrate proteins in the nanocage of groel. *Biochemistry.* 60:460–464.
61. Korobko, I., H. Mazal, …, A. Horovitz. 2020. Measuring protein stability in the GroEL chaperonin cage reveals massive destabilization. *eLife.* 9:e56511.
62. Sameshima, T., R. Iizuka, …, T. Funatsu. 2010. Denatured proteins facilitate the formation of the football-shaped GroEL–(GroES) 2 complex. *Biochem. J.* 427:247–254.
63. Takei, Y., R. Iizuka, …, T. Funatsu. 2012. Single-molecule observation of protein folding in symmetric GroEL-(GroES) 2 complexes. *J. Biol. Chem.* 287:41118–41125.
64. Ye, X., and G. H. Lorimer. 2013. Substrate protein switches GroE chaperonins from asymmetric to symmetric cycling by catalyzing nucleotide exchange. *Proc. Natl. Acad. Sci. USA.* 110:E4289–E4297.
65. Yang, D., X. Ye, and G. H. Lorimer. 2013. Symmetric GroEL:GroES2 complexes are the protein-folding functional form of the chaperonin nanomachine. *Proc. Natl. Acad. Sci. USA.* 110:E4298–E4305.
66. Llorca, O., S. Marco, …, J. M. Valpuesta. 1994. The formation of symmetrical GroEL-GroES complexes in the presence of ATP. *FEBS Lett.* 345:181–186.
67. Corrales, F. J., and A. R. Fersht. 1996. Kinetic significance of groel14·(groes7) 2 complexes in molecular chaperone activity. *Folding Des.* 1:265–273.
68. Fei, X., D. Yang, …, G. H. Lorimer. 2013. Crystal structure of a GroEL-ADP complex in the relaxed allosteric state at 2.7 Å resolution. *Proc. Natl. Acad. Sci. USA.* 110:E2958–E2966.
69. Fei, X., X. Ye, …, G. H. Lorimer. 2014. Formation and structures of groel:groes2 chaperonin footballs, the protein-folding functioal form. *Proc. Natl. Acad. Sci. USA.* 111:12775–12780.

70. Stan, G., G. H. Lorimer, …, B. R. Brooks. 2007. Coupling between allosteric transitions in GroEL and assisted folding of a substrate protein. *Proc. Natl. Acad. Sci.* 104:8803–8808.

71. Kirkpatrick, S., C. D. Gelatt, Jr., and M. P. Vecchi. 1983. Optimization by simulated annealing. *Science.* 220:671–680.

72. Evans, M. R., and S. N. Majumdar. 2011. Diffusion with stochastic resetting. *Phys. Rev. Lett.* 106:160601.

73. Pal, P. S., A. Pal, …, J. S. Lee. 2023. Thermodynamic trade-off relation for first passage time in resetting processes. *Phys. Rev. E.* 108:044117.

74. Mugnai, M. L., C. Hyeon, …, D. Thirumalai. 2020. Theoretical perspectives on biological machines. *Rev. Mod. Phys.* 92:025001.

75. Song, Y., and C. Hyeon. 2021. Thermodynamic uncertainty relation to assess biological processes. *J. Chem. Phys.* 154:130901.

76. Frank, G. A., M. Goomanovsky, …, G. Haran. 2010. Out-of-equilibrium conformational cycling of GroEL under saturating ATP concentrations. *Proc. Natl. Acad. Sci. USA.* 107:6270–6274.

77. Kim, S. H., and T. R. Cech. 1987. Three-dimensional model of the active site of the self-splicing rRNA precursor of Tetrahymena. *Proc. Natl. Acad. Sci.* 84:8788–8792.

78. Michel, F., and E. Westhof. 1990. Modelling of the three-dimensional architecture of group I catalytic introns based on comparative sequence analysis. *J. Mol. Biol.* 216:585–610.

79. Lehnert, V., L. Jaeger, …, E. Westhof. 1996. New loop-loop tertiary interactions in self-splicing introns of subgroup IC and ID: a complete 3D model of the Tetrahymena thermophila ribozyme. *Chemistry & biology.* 3:993–1009.

80. Doudna, J. A., and T. R. Cech. 2002. The chemical repertoire of natural ribozymes. *Nature.* 418:222–228.

81. Rangan, P., B. Masquida, …, S. A. Woodson. 2003. Assembly of core helices and rapid tertiary folding of a small bacterial group I ribozyme. *Proc. Natl. Acad. Sci. USA.* 100:1574–1579.

82. Grohman, J. K., M. Del Campo, …, R. Russell. 2007. Probing the mechanisms of DEAD-box proteins as general RNA chaperones: the C-terminal domain of CYT-19 mediates general recognition of RNA. *Biochemistry.* 46:3013–3022.

83. Jarmoskaite, I., P. Tijerina, and R. Russell. 2021. ATP utilization by a DEAD-box protein during refolding of a misfolded group I intron ribozyme. *J. Biol. Chem.* 296:100132.

84. Bhaskaran, H., and R. Russell. 2007. Kinetic redistribution of native and misfolded RNAs by DEAD-box chaperone. *Nature.* 449:1014–1018.

85. Sujatha, P. K., and S. A. Woodson. 2004. Intracellular folding of the Tetrahymena group I intron depends on exon sequence and promoter choice. *RNA.* 10:1526–1532.

86. Jackson, S. A., S. Koduvayur, and S. A. Woodson. 2006. Self-splicing of a group I intron reveals partitioning of native and misfolded RNA populations in yeast. *RNA.* 12:2149–2159.

87. Shiraishi, N., K. Saito, and H. Tasaki. 2016. Universal trade-off relation between power and efficiency for heat engines. *Phys. Rev. Lett.* 117:190601.

88. Pietzonka, P., and U. Seifert. 2018. Universal trade-off between power, efficiency, and constancy in steady-state heat engines. *Phys. Rev. Lett.* 120:190602.

89. Dechant, A., and S.-ichi Sasa. 2018. Entropic bounds on currents in langevin systems. *Phys. Rev. E.* 97:062101.

90. Hwang, W., and C. Hyeon. 2018. Energetic costs, precision, and transport efficiency of molecular motors. *J. Phys. Chem. Lett.* 9:513–520.

91. Barato, A. C., and U. Seifert. 2015. Thermodynamic Uncertainty Relation for Biomolecular Processes. *Phys. Rev. Lett.* 114:158101.

92. Seifert, U. 2019. From stochastic thermodynamics to thermodynamic inference. *Annu. Rev. Condens. Matter Phys.* 10:171–192.

93. Matthew, P. L., and D. A. Sivak. 2024. Flow of energy and information in molecular machines. *Annu. Rev. Phys. Chem.* 76

94. Fayet, O., T. Ziegelhoffer, and C. Georgopoulos. 1989. The groES and groEL heat shock gene products of Escherichia coli are essential for bacterial growth at all temperatures. *J. Bacteriol.* 171:1379–1385.

95. Fayer, O., J.-M. Louarn, and C. Georgopoulos. 1986. Suppression of the Escherichia coli dnaA46 mutation by amplification of the groES and groEL genes. *Mol. Gen. Genet. MGG.* 202:435–445.

96. Van Dyk, T. K., A. A. Gatenby, and R. A. LaRossa. 1989. Demonstration by genetic suppression of interaction of GroE products with many proteins. *Nature.* 342:451–453.

97. Gordon, C. L., S. K. Sather, …, J. King. 1994. Selective in vivo rescue by GroEL/ES of thermolabile folding intermediates to phage P22 structural proteins. *J. Biol. Chem.* 269:27941–27951.

98. Bershtein, S., W. Mu, …, E. I. Shakhnovich. 2013. Protein quality control acts on folding intermediates to shape the effects of mutations on organismal fitness. *Mol. Cell.* 49:133–144.

99. Rudan, M., D. Schneider, …, A. Krisko. 2015. RNA chaperones buffer deleterious mutations in E. coli. *eLife.* 4:e04745.

100. Braxton, J. R., H. Shao, …, D. R. Southworth. 2024. Asymmetric apical domain states of mitochondrial hsp60 coordinate substrate engagement and chaperonin assembly. *Nat. Struct. Mol. Biol.* 31:1848–1858.

101. Sun, Y., and S. A. Woodson. 2025. Disassembly of unstable RNA structures by an E. coli DEAD-box chaperone accelerates ribosome assembly. *Nucleic Acids Res.* 53:gkaf104.